Glasses: Chalcogenides

Myungkoo Kang, University of Central Florida, Orlando, FL, United States
Kathleen A Richardson, University of Central Florida, Orlando, FL, United States

Introduction

Chalcogenide glasses (ChGs) have received increasing global interest over the past decade due to their suitability for use in infrared (IR) systems (Zhang *et al.*, 2003; Eggleton *et al.*, 2011; Parvanov *et al.*, 2008; Sanghera and Aggarwal, 1999; Zhang *et al.*, 2004). With compositional tuning, their transparency can extend over the full IR spectral range (Zhang *et al.*, 2003; Eggleton *et al.*, 2011; Parvanov *et al.*, 2008; Sanghera and Aggarwal, 1999; Zhang *et al.*, 2004; Buff, 2016; Sisken, 2017; Yadav *et al.*, 2017; Goncalves *et al.*, 2018). Unlike oxide glasses (which have oxygen as a key anionic constituent), ChGs are part of a class of "non-oxide" glasses. This lack of oxygen (O) is important to their use and makes them transparent throughout the IR. Since most metal (M)-O species possess resonance absorption bands in the IR, the removal of oxygen, along with the removal of other potentially absorbing impurities (such as moisture (hydroxide, OH^-, water, H_2O) and hydrides (M-H)) and any residual particulate from the melting process, is critical in ultimately defining the glass' resulting transparency. Like halides (glasses based on group VII species), chalcogen (Ch) species (based on group VI elements) combine with other chalcogens or metalloids such as As, Sb, Ge and Ga, to form stable glasses with wide (compositionally-specific) glass forming regions. However, the bonds formed in these glasses are much weaker than M-O bonds and thus ChGs typically are softer, less chemically stable and have lower melting/softening temperatures as compared to oxide glasses. Additionally, due to the bonding present, ChGs can exhibit metastable properties including photosensitivity (radiation-induced structural modification) which varies both with glass composition and the material's bandgap (defined by the bonds present) and type of exciting radiation (Kolobov and Tominaga, 2012). While these glass attributes may limit the material's use in some instances, they can also be exploited to extend their use towards the realization of unique optical or physical property functionality (Carlie *et al.*, 2010). There are several excellent reviews on the basic attributes of ChGs for the interested reader that cover these topics (Hilton, 2010; Seddon *et al.*, 2006; Kolobov and Tanaka, 2001; Wang, 2014; Adam and Zhang, 2014; Richardson and Kang, 2020).

While ChGs and related alloys have been extensively studied since the early 1960s, there remains relatively few commercial products based on these glasses. Those that are available were largely developed in the 1960–1970 time frame, for xerographic and other bulk optical applications (Bixby and Ullrich (1956); Texas Instruments (1967)). Hence, these compositions are no longer protected by patents and hence are known by varying product names, manufactured by multiple vendors, such as Amorphous Materials, Umicore, Vitron, and SCHOTT AG. While ChGs were being developed internationally during this time, an excellent review of the history of the effort in the US starting at Texas Instruments and then at Amorphous Materials, including details of early glass development, melting methods, and glass properties, can be found in Hilton (2010). An additional source of data on numerous ChGs developed and/or measured in Russia can be found in Kokorina (1996). While the history of ChGs is rich, the small number (currently 6) of commercially produced compositions is largely due to limited demand of these glasses which until recently, have only been employed in a few *bulk* optical applications (such as in lenses for IR imaging systems). The most common of these has been in IR vision systems (so-called "forward looking IR" or FLIR systems) that allow vision in dark or foggy systems while driving. More recently, use of these glasses in commercial systems such as iPhones has broadened their use and familiarized the public with technology that was previously used solely by the military. Hence, efforts to scale the manufacturability of the glasses to include their forming into suitable, low cost lens elements and systems has led to wide scale academic and industrial work in techniques such as precision glass molding (PGM).

With expanded interest in sensing, security and imaging since 2010, the market for low cost alternatives to expensive crystalline optics such as Ge and Si, has invigorated ChG research efforts worldwide. This common "chicken and egg" conundrum exists for these IR materials, in that, without sufficient chemistry-structure-property data on candidate glasses that can be scaled to commercially-relevant sizes, optical designers cannot put these media into optical design codes that make the scale-up and commercialization of the new compositions economically viable. This blockage, however, has started to ease in recent years, as new data has been published by many groups who have worked to extend lab-scale melts to commercially viable sizes (Gibson *et al.*, 2019). Here, important characteristics required for data sheets include the glass' transition temperature (T_g), refractive index (n) and its variation with wavelength, ($dn/d\lambda$) or temperature (dn/dT) along with the glass' viscosity (η) and coefficient of thermal expansion, (CTE). All of these properties are composition specific, challenging to produce with superb repeatability unless made in controlled large scale melting production, and expensive to measure. Additionally, applications may or may not require ultra-high purity for low loss applications at specific wavelengths, and this requirement entails additional processing and cost consideration. Hence, unlike oxide glasses where most of these hurdles have been overcome in the $\sim$100 years that companies have been making those glasses, these challenges still impede production and adoption of new ChG compositions into optical systems. Hence, as optical design teams work to integrate promising candidate materials into new, higher volume optical designs, this will reinforce the need of new glasses and encourage market attractiveness to glass producers.

This article discusses glasses and composites based on glasses, multi-phase (glass + crystalline) media where controlled crystallization has been employed to extend their properties towards use as glass ceramics (GCs). For brevity, we confine our discussion to the use of ChGs or GCs to optical applications, with reference to very recent advances in applications where these materials are passive (i.e., examples where the ChG does not contain a rare-earth or transition metal dopant for luminescence purposes). Highlighted in the article are examples of how ChGs can be tuned through composition (glass' chemical constituents), morphology (the glass' homogeneous or phase separated nature), and microstructural modification associated with the controlled nucleation and growth of nanocrystal phases within the parent glass matrix to realize novel functionality (Buff, 2016; Sisken, 2017; Yadav *et al.*, 2017; Richardson, 2018; Li *et al.*, 2014; Yang *et al.*, 2007; Wang *et al.*, 2009; Zhao *et al.*, 2005; Xia *et al.*, 2006; Sisken *et al.*, 2019; Kang *et al.*, 2018a,b; Richardson *et al.*, 2016; Yadav *et al.*, 2019). Briefly discussed is a short summary on the state of the art in exploiting these compositionally defined attributes to enable low cost lenses created via PGM. This article discusses key material attributes to ChGs' and ChG-based GCs' for use in the IR. Specifically highlighted are uses in applications for the mid-wave IR (MWIR) spectral region in applications such as low cost lenses via PGM, fibers (communication) and introduces recent progress on new opportunities such as gradient index optics (imaging), low-loss waveguides (signaling), and optical nonlinearity (sensing and lighting).

ChGs: For Bulk Media and Fibers

Processing Characteristics of ChGs

ChGs are amorphous, non-crystalline solids formed largely by the fusion process (often called the melt-quench process) whereby elemental starting materials from group VI and other metalloids are combined and melted in a sealed quartz ampoule prior to homogenization, quenching and annealing. Unlike oxide glasses which can be melted in open crucibles, the high vapor pressures of chalcogen species such as sulfur or selenium, require melting in a sealed container. While melting in a fused silica ampoule may introduce minor oxide impurities to the melt (and for some applications is unacceptable), this trace level of contamination comes with the added benefit of poor wetting. As shown in **Fig. 1**, this enables melted ChG "rods" to be seamlessly released from their crucible with minimal sticking. Sulfide glasses and glasses containing alkali tend to react more with the crucible and in these melts, ampoules are often coated with carbon to minimize interaction and adhesion (Martin and Bloyer, 1990). Such optimization has been shown especially useful in the examination of ChGs for battery applications where doping with Na or Li requires shielding from interaction with the glass crucible ampoule. Such processing considerations are required in the melting of these glasses as their properties can be adversely influenced by such melting environment variables that impact glass properties and crystallization stability.

Crystallization Stability and Compositional Trends

A glass' network structure is defined by its thermal history, i.e., the path that the melt takes from the liquidus melt to form a solid at room temperature. How that glass structure organizes is influenced by the cooling rate used and thus bulk glasses require annealing as their large aspect ratios (interior versus exterior skin) can see vastly different cooling rates that can induce stress and stress birefringence. This volume effect is much less pronounced in the thin diameters of optical fibers where cooling rates are very high. Despite the low thermal conductivities of glass, most fibers do not possess excessive density variation due to forming temperature gradients that degrades their refractive index homogeneity if the preform is compositionally homogeneous. Such thermal history and the distance the glass network is from its "equilibrium state" (for purposes of this discussion, not the state of the equivalent crystal, but that of a well-annealed bulk glass) will impact the resulting glass' properties as well if cooling was sufficient to avoid the nucleation and growth associated with crystallization. Crystallization in all glasses, but especially in fibers, leads to both absorption and scatter loss and thus, needs to be avoided. Various reviews on crystallization behavior in ChGs have been made (Hari *et al.*, 1998), and a subset of topics important to fibers are discussed in more detail here.

Crystallization in glass relies on nucleation and subsequent growth of crystals. Without the formation of stable nuclei, subsequent crystallization cannot occur. Crystallization in glass, in most cases, is undesirable and this is especially true in bulk optical

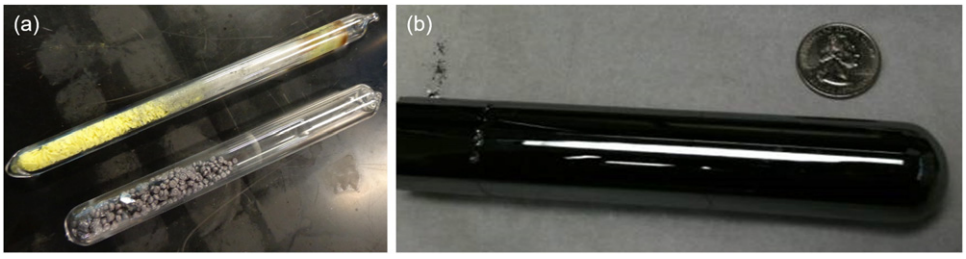

Fig. 1 A batched sulfide (yellow) and selenide (black) ChG prior to melting in a sealed ampoule (a); a 250 g rod of selenide glass after melting (b); shown as a reference for size is a US quarter.

glass and glass fibers where the presence of crystallites can result in scattering loss due to refractive index mismatch. To understand the key conditions of crystallization which must be avoided to ensure low optical loss fibers, one must be familiar with the temperature dependence of both nucleation process in ChGs and the subsequent growth of crystals should stable nuclei form. Stability against crystallization is often inferred by the difference between T_x, the onset of measured crystallization in a glass as indicated by exothermic heat release during thermal analysis measurement (such as differential scanning calorimetry, DSC) and the material's glass transition temperature, T_g. When this temperature difference, ΔT, exceeds $\sim 100^{\circ}C$, it is generally considered that a glass can successfully be formed into fibers, avoiding crystallization. Since non-oxide glasses typically have T_g's much lower than oxide glasses, an estimated ΔT provides an initial insight on how composition, dopant type, and concentration can impact crystallization stability and the probability of being able to fabricate low loss optical fiber. However, a variety of historic references to measurement of critical cooling rates (CCR) of chalcogenide melts as a function of composition (Kokorina, 1996; Mikhailov and Tver'yanovick, 1986) and the role of variation in annealing protocols on refractive index provides insight into the intricacies of such measurements.

It is sometimes difficult to compare compositional dependency of ChG stability across authors, as measurements of ΔT are dependent on measurement heating rate used, which may not always be reported. However, it is useful to see the role compositional variation (rather than configurational variation) plays in glass stability. To illustrate the trend, a common set of glass systems is compared, as shown in **Fig. 2** (Adam and Zhang, 2014). Here, two families of $Ge_{28}(As/Sb)_{12}(S_x/Se_{60-x})$ are compared for their stability, ΔT illustrating that stability is largely dominated by chemical rather than configurational effects. In these glasses, only isostructural substitutions have been made to the glass network (as both As and Sb have a CN = 3) and S and Se are both two-coordinated. Hence, the network role of the chemical constituents in these two glass families (comparing As and Sb) are similar, but the magnitude of stability is defined by the type of the lower coordinated species (S or Se) and its quantity. Fibers based on Ge–As–Se–Te glasses have shown some of the lowest losses in ChG fibers investigated and it largely can be attributed to the glass' crystallization stability. As discussed by Shiryaev *et al.* (2004), $Ge_xAs_{40-x}Se_{40}Te_{20}$, where x = 0–40, exhibit T_g that ranges from 140 to 320°C depending on Ge content and heating rate. Glasses with less than 35 mol% Ge showed no exothermic features associated with crystallization, indicating impressive high glass stability. Glasses within the ranges of Ge: 6–24 at% and Te: 42–48 at% were shown to have T_g above 200°C with no sign of crystallization during annealing for 20 h at temperatures exceeding T_g by 50–100°C (Tikhomirov *et al.*, 2004).

Nucleation and growth theory can be applied to ChG materials for a variety of fundamental and applied reasons. A summary of these theories and methods to calculate nucleation and growth rates from experimental data (as specifically applied to Tellurite glasses) can be found in Massera (2009). The same protocols have been employed to ChGs as discussed below, to realize optical glass ceramics, where the secondary crystalline phase has a refractive index match to the parent glass to minimize loss. Examples of controlled crystallization in ChGs have been shown to be effective in realizing bulk glass ceramics (to either enhance thermal or mechanical stability (Sharma *et al.*, 2020)), create gradients in refractive index (GRIN) (Richardson, 2018; Sisken, 2017; Kang *et al.*, 2018a,8b; Kang *et al.*, 2020a,b) or in commercial products resulting in optical memories based on GeSbTe phase change media (PCM) (Adam and Zhang, 2014; Zhang *et al.*, 2019). Recently, efforts to tailor crystalline phase formation in reversible, low optical loss PCMs for conformal coatings and the formation of permanent optical function realized through optical nanocomposites in bulk and films of ChG have shown that both compositional tuning and the associated understanding of crystal nucleation and growth kinetics can be exploited for new optical applications (Kolobov and Tominaga, 2012; Kolobov and Tanaka, 2001; Richardson and Kang, 2020; Bixby and Ullrich, 1956; Texas Instruments, 1967; Gibson *et al.*, 2019; Richardson, 2018; Kang *et al.*, 2019; Mingareev *et al.*, 2019). Here, tailoring of physical properties through the controlled formation and growth of specific

Composition	T_g (K)	T_x (K)	ΔT (K)
$Ge_{28}Sb_{12}S_{60}$	615	800	185
$Ge_{28}Sb_{12}S_{45}Se_{15}$	596	784	188
$Ge_{28}Sb_{12}S_{30}Se_{30}$	592	766	174
$Ge_{28}Sb_{12}S_{15}Se_{45}$	595	770	175
$Ge_{28}Sb_{12}Se_{60}$	571	764	194
$Ge_{28}As_{12}S_{60}$	678	698	120
$Ge_{28}As_{12}S_{45}Se_{15}$	660	789	129
$Ge_{28}As_{12}S_{30}Se_{30}$	651	784	134
$Ge_{28}As_{12}S_{15}Se_{45}$	649	782	133
$Ge_{28}As_{12}Se_{60}$	615	778	163

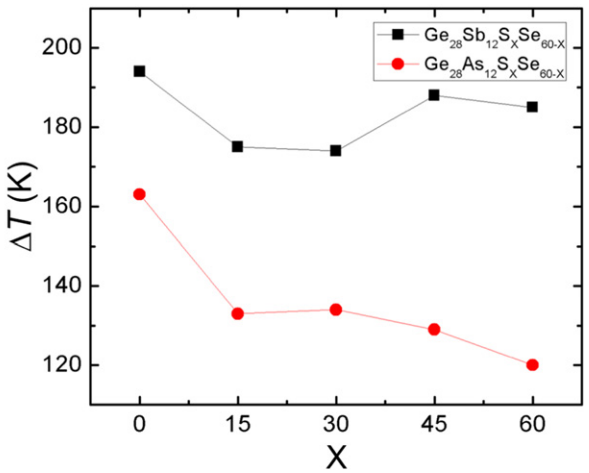

Fig. 2 (Left) glass transition and crystallization temperatures, with corresponding stability windows, for two families of ChGs, (right) ΔT versus S/Se ratio for $Ge_{28}(As/Sb)_{12}(S_x/Se_{60-x})$ plotted based on the tabulated table. Reproduced with permission from Adam, J.L., Zhang, X., 2014. Chalcogenide Glasses: Preparation, Properties and Applications. Woodhead Publishing Limited. Copyright 2014 Elsevier.

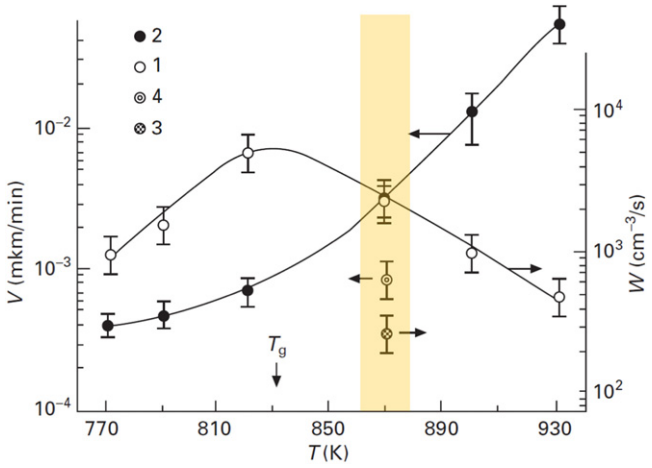

Fig. 3 Temperature dependence of nucleation and growth rates in undoped (data sets 3 & 4) and doped (data sets 1 & 2) Pr:$(Ga_2S_3)_{0.7}(La_2S_3)_{0.3}$ glass. The shaded region illustrates the increase (note logarithmic scale) in both nucleation (W) and growth (V) rates with Praseodymium doping level in the glass matrix.

secondary crystalline phases with defined volume fractions can lead to optical function not realized in static glass or crystalline media.

In fibers, crystalline phase formation is largely undesirable and thus, should be avoided. Knowledge of a glass' nucleation and growth rates provides quantitative insight into this process. The formation of rate versus temperature plots for both nucleation and growth (referred to by either *I* or *W* to denote nucleation rates and *V* or *U* to define growth rates) provides insight not only on the temperatures where crystal nuclei can form, but also at what temperature they grow and at what rate. Clearly, for most optical fiber glass compositions, one desires to operate in temperature regimes where a glass' nucleation rate is very low, and the growth rate for any small concentration of nuclei present approaches zero. This is the target for creating crystallite-free fibers. However, should one want to "selectively" create (or sustain) a nanocrystalline phase within the candidate glass system, knowledge of a glass' *I-U* curve and its use in defining optimal draw conditions will indicate what extent of crystallite formation and/or growth might occur. The selective use of this strategy for engineering controlled crystallization in tellurite cladding glasses showed that nanocrystal phase formation, known to enhance mechanical properties, was an efficient means to strengthen the outer layer of fibers formed in these typically crystallization-prone glasses (Massera *et al.*, 2010a,b).

Crystallization stability can be influenced not only by network constituents, but also by dopants. The variation in nucleation and growth behavior with doping is especially important when considering compositional selection of rare-earth doped ChGs such as in the development of active media. Since fibers of active, rare earth doped ChGs are one of the leading areas of interest for their use (Richardson and Kang, 2020), we highlight here this effect as example. The impact on both the nucleation and growth behavior of the glass with addition of the rare earth dopant praseodymium is noted in the study by Dianov *et al.* (1997). While illustrated in one ChG composition GaLaS, the impact on both the nucleation and linear growth rate with Pr doping is clear. **Fig. 3** shows the variation (data set 1 and 2) in nucleation (*W*) and growth (*V*) for Pr:$(Ga_2S_3)_{0.7}(La_2S_3)_{0.3}$ glass as a function of temperature (*K*) as compared to the undoped material (data set 3 and 4). At the common temperature of 870K (highlighted with gray shading), comparing the rates for nucleation and growth, one observes that as compared to the undoped glass, the doped glass exhibits an almost 10-fold increase in nucleation rate, along with a concurrent increase in growth rate (approximated to $\sim 200\times$). These data suggest that the dopant's presence in the glass network increases the likelihood that stable nuclei will form and once formed, will grow at a faster rate. This infers that measurement of nucleation and growth rates on actual compositions is needed to inform the expected crystallization stability of the material upon fiberization.

Viscosity (η) and Temperature (T) Dependence

A glass' viscosity (η, in units of Pa s) and temperature (T) dependence is a material-specific attribute, defined by the bonding in the glass matrix and to first order, the glass' average bond strength. For ChGs, this attribute is especially important in applications such as precision glass molding (PGM) and in the drawing of optical fibers. Defining the suitable fiber draw conditions (draw temperature and draw rate) is a fairly straight forward process when a glass' viscosity- temperature (η-T) behavior is known. Since core and cladding glasses should have similar T_g and CTE behavior to ensure compatibility during drawing, it is assumed that the η-T response of these two glasses, while differing slightly in index, will be close in both their thermal position (lateral shift) and curve steepness. These attributes of a η-T curve and its shape are important as they determine whether the glass has a short (steep) slope or long (less steep) range of processing temperatures. This short/long nomenclature is often used to highlight the ease (long) or difficulty (short) by which a glass can be fiberized as these terms define the temperature required for both flow and sometimes avoidance of crystallization. A similar η-T behavior between core and clad glass allows fiber drawing with minimal interface defects

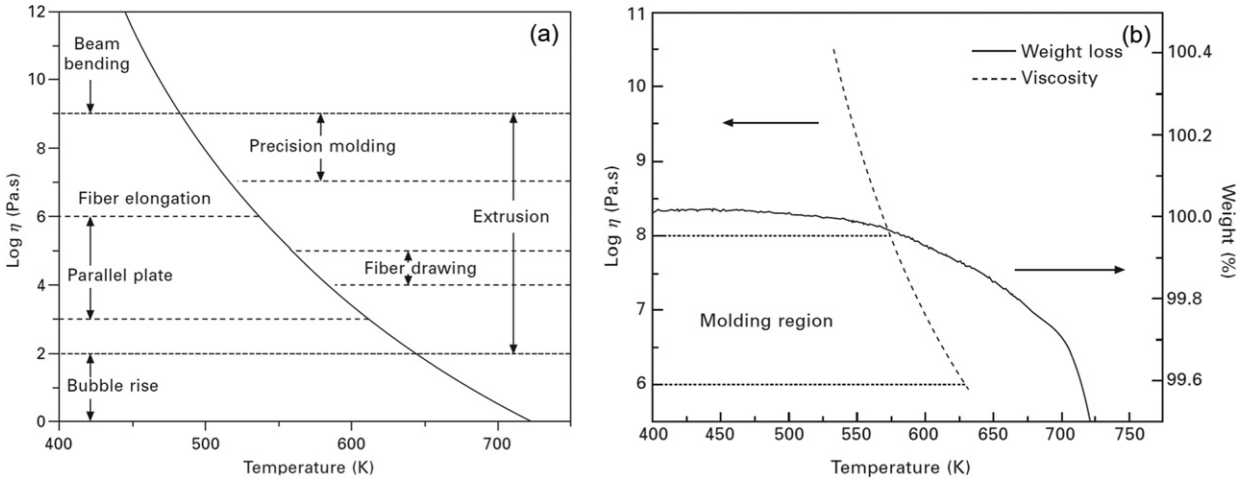

Fig. 4 (a) An overview of the viscosity regions for a ChG, showing the ranges for measurements [left] and hot-forming applications [right], (b) a comparison of the viscosity and volatilization curves for $Ge_{10}As_{40}Se_{50}$ glass showing evidence of out-gassing in the molding region. Reproduced with permission from Adam, J.L., Zhang, X., 2014. Chalcogenide Glasses: Preparation, Properties and Applications. Woodhead Publishing Limited. Copyright 2014 Elsevier.

(bubbles, trapped gas, or micro-delamination). Such defects would compromise (increase) the measured loss of the fiber. The literature contains multiple examples of such data for some ChG compositions, but as it is a time-consuming and instrumentation-specific measurement to make. Hence, such data are often not reported for more exotic or exploratory glasses as considerable measurement and specific sample fabrication are required and exploratory melts are frequently small in volume and not homogeneous.

Measurements of thermal properties including glass viscosity behavior as a function of composition is well studied. A detailed discussion of experimental methods and typical thermal behavior in ChGs is reviewed in Adam and Zhang (2014). **Fig. 4(a)** highlights the key thermal signature regimes for viscosity illustrating the measurement methods (left side of **Fig. 4(a)**) and the typical glass processing windows for typical glass manufacturing protocols (right side of **Fig. 4(a)**). Of relevance to the topic of ChGs for fibers are the temperature range for extrusion (10^2–10^9 Pa s) such as that for forming extruded rods or cane and that for fiber drawing (10^4–10^5 Pa s). These ranges will vary with composition and may vary with individual fiber drawing apparatus, but are generally accepted as a guide to predicting variation in formation behavior with composition. **Fig. 4(b)** overlays a η-T curve for a GeAsSe glass with a thermogravimetric spectrum that defines the weight loss of that glass with temperature. Shown in the figure is evidence that the onset of volatilization of glass constituents occurs near the low temperature range of precision glass molding. As compared to the data shown in **Fig. 4(a)**, this temperature range is below the temperature range where fiberization for this glass takes place (at $\eta \sim 10^4$–10^5 Pa s), thus suggesting that compositional variation during drawing could occur without strict temperature control. Such compositional variation (volatilization) could lead to accompanying refractive index variations if special care is not taken to control temperature excursions for ChGs.

Fig. 5 illustrates how a characteristic viscosity-temperature curve varies with composition for a simple binary As–Se glass (Musgraves *et al.*, 2011). This plot is illustrative of the correlation between glass fluidity and network structure. Several key points are important to highlight when evaluating viscosity in ChG glasses by multiple experimental (such as by beam bending viscosity (BBV) – shown as the lower temperature data points and parallel plate viscometry (PPV) – shown as the upper temperature data points). Not shown are points defined by the fiber elongation method which requires fibers to be formed and measured using a specialized set up to yield data through the region ($\sim 10^{7.6}$ Pa S). Firstly, while there are varying discussions on the best means to "fit" experimental data (Mauro *et al.*, 2016), most literature data employ the Vogel-Fulcher-Tahmann (VFT) method. The steepness of the viscosity curve is indicative of the working range available to draw, but the lateral position (in temperature) provides a gauge of the variation in energy needed to sever the structural units present to initiate flow. Glasses to the left in the series have much lower three-coordinated As present and thus a higher Se content which in this binary system, forms rings and chains of Se. Se–Se bonds are have a lower bond energy than As–Se bonds and thus, these higher Se content glasses see an onset of flow at lower temperatures. The similarity in the shape of the series of curves is testament to the structural role of the primary bonds, found in the $AsSe_{3/2}$ pyramidal units that make up the "building blocks" in this glass and the Se_n chains that interconnect the pyramids. $As_{40}Se_{60}$, the stoichiometric glass contains only interconnected pyramidal units and no homopolar Se–Se bonds.

These data are especially important when considering the formation of low cost optics such as lenses prepared by a precision glass molding (PGM) technique. Often simply referred to as "molding", the primary objective is that the glass be sufficiently stable to crystallization (have a high ΔT) to not devitrify upon the reheating cycle that accompanies the molding process. Secondarily, it is desirable that a suitably short (and thus cost-effective) molding cycle be created whereby glass can be loaded into a molding machine, rapidly heated to a suitable molding temperature (as defined by its viscosity such as shown in **Figs. 4(a)** and **5**), be fluid enough at that temperature to form a desired shape under an applied load, then be cooled such that the load can be

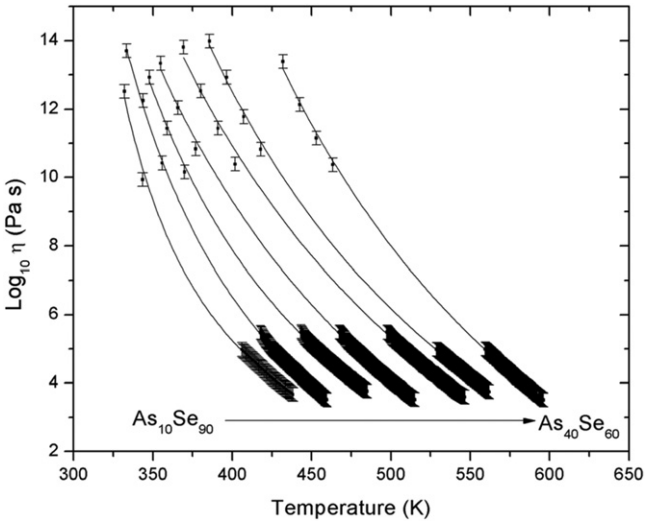

Fig. 5 Viscosity curves for the As_xSe_{100-x} glass family from x = 10 (left-most) to x = 40 (right-most) obtained through beam bending and parallel plate viscometry. Reproduced with permission from Musgraves, J.D., Wachtel, P., Novak, S., Wilkinson, J., Richardson, K., 2011. Composition dependence of the viscosity and other physical properties in the arsenic selenide glass system. J. Appl. Phys. 110, 063503. Copyright 2011 AIP.

released and the cooled lens can be ejected from the machine. While simple in principal, the process is complex as there are various levels of property changes imparted to the glass by this "new" thermal history. Not only does the glass network structure change, but so too does its density, refractive index and, depending on composition, other aspects such as relaxation phenomena. Here, a glass' network undergoes time dependent changes with temperature. Since ChGs have T_g which in some cases are as low as ~100–200°C above room temperature, there exists enough thermal driving force at room temperature, to cause time dependent variations in properties with time at room temperature. This is important in systems that must perform over a range of temperatures where the change in an optical system's focus, needs to remain stable. This effect has been studied in a variety of publications, which have been summarized for a variety of ChGs in Koontz (2014). Hence, while interesting and more widely applied for a wide variety of ChGs being employed in low cost IR imaging systems, molded IR optics still require optimization for specific commercial applications where their thermal and physical properties play a guiding role.

Novel Optical Function and Gradient Properties

The above discussions highlight properties of ChGs which like other oxide and halide glasses, are important for their use as glasses or glass ceramics and how these properties often impact their manufacturability. Discussed in subsequent sections is how one can exploit some of the common misconceptions of ChGs towards generating unique function. Often, ChGs are seen as "limited" in their use due to their bonding and the impact of this on function. As discussed by Carlie *et al.* (2010), this "perceived" set of limitations (low T_g, weak (er) bonds, low chemical durability, poor thermal stability) can be used towards deliberate modification of any physical properties. In the remainder of this article, we focus on such knowledge to optimized aspects of optical function in ChGs.

GRIN via Spatially Controlled Nucleation and Growth

To control and manipulate light propagation in bulk imaging systems, multiple optical components are selected and combined to realize the desired optical function, across a defined spectral window. Here, individual IR optical components comprised of varying optical materials (glasses, crystals, and semiconductors) are often fabricated into complex, non-planar geometries exploiting their unique optical properties (Zhang *et al.*, 2003; Cha *et al.*, 2012; Hisakuni and Tanaka, 1995; Ramachandran *et al.*, 1997; Beadie *et al.*, 1998; Saitoh and Tanaka, 2003; Sanchez *et al.*, 2011; Kumaresan *et al.*, 2013). Legacy optical design and fabrication strategies often require costly multi-step manufacturing processes which limit system design flexibility, and this can lead to an increase in the size, weight, and power consumption (SWaP) potentially impacting both the performance and/or cost of the resulting imaging system (Zhang *et al.*, 2003; Cha *et al.*, 2012; Hisakuni and Tanaka, 1995; Ramachandran *et al.*, 1997; Beadie *et al.*, 1998; Saitoh and Tanaka, 2003; Sanchez *et al.*, 2011; Kumaresan *et al.*, 2013; Booth, 2014). These issues can be significant in bulk IR systems where high density crystalline materials are widely used, as these optical materials possess monochromatic/chromatic aberrations and/or limitations in performance at elevated temperatures (Moore, 1980; Li, 1980). Next-generation imaging systems will require materials with enhanced multi-spectral or broadband optical functionality, thus further challenging the aim to reduce the number of components in an optical system and resulting platform footprint. Reducing SWaP in optical

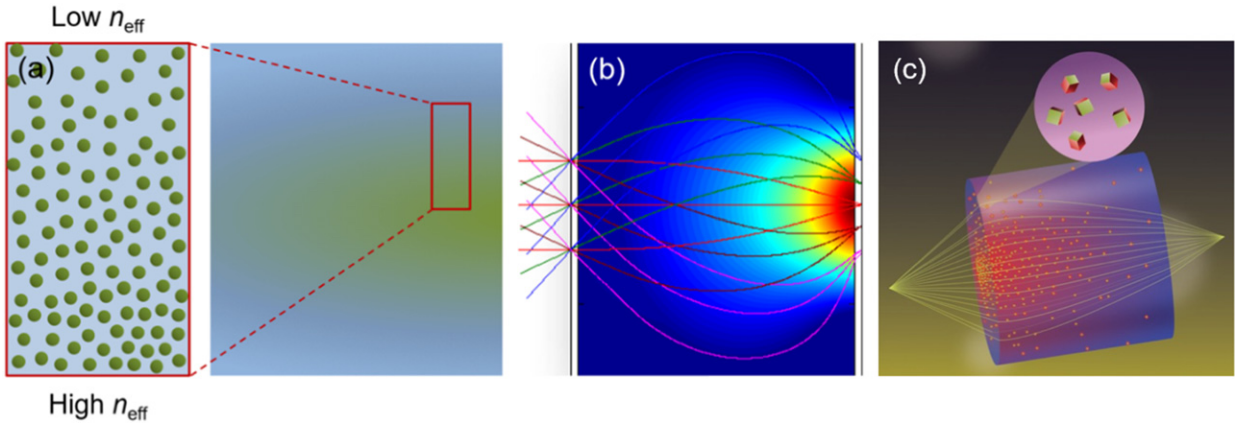

Fig. 6 (a) a GRIN medium where the density of high-index nanocrystals (green) are spatially varied within a low-index matrix (blue), (b) ray tracing through a resulting flat lens, and (c) a 3-D view of the flat lens where high-index nanocrystals' distribution, a GRIN profile, and ray tracing are shown. Reproduced with permission from (c) Kang, M., Sisken, L., Lonergan, C., *et al.*, 2020b. Monolithic chalcogenide optical nanocomposites enable infrared system innovation: Gradient Refractive Index (GRIN) optics. Adv. Opt. Mater. 8, 2000150. Copyright 2020 Wiley.

systems through the creation and use of IR nanocomposite materials possessing GRIN profiles provides a viable solution to this challenge (Moore, 1980). Here the optical composite, in the form of a bulk component or planar waveguide, can yield a uniquely tailorable solution exploiting tunable optical function created by combining the desirable attributes of effective media. A key strategy to create GRIN profiles within a single medium involves spatial control of a high refractive index phase in a medium. Conversion of a base glass to a glass-ceramic where the spatial variation in the volume fraction of high index nanocrystallites in a low index base glass can be tailored results in a transparent GRIN effective medium, as illustrated in **Fig. 6(a)–(c)** (Richardson, 2018; Richardson *et al.*, 2016; Kang *et al.*, 2020a,b). This technique provides a novel method to both miniaturize and enhance current IR components over that realized solely on homogeneous, single phase spherical or aspherical lenses thereby enabling a flat lens with a low chromatic aberration and a substantially reduced SWaP.

Bulk GRIN Materials

Recently, it has been reported that $GeSe_2$–As_2Se_3–PbSe (GAP–Se) ChGs with PbSe content of ~10–45 mol% in their bulk form are spontaneously separated into Pb-rich and Pb-deficient amorphous phases upon standard melt-quench protocol, as shown in **Fig. 7(a)** and **(b)** (Goncalves *et al.*, 2018). The energetically-favorable route to phase separation consistently seen in this material system has gained interest from optical designers and glass scientists since the Pb-rich amorphous phases, once thermally treated, can be exclusively converted into nanocrystallites with an index greater than that of the surrounding matrix. This matrix remains amorphous, as evidenced by bright and dark field (BF and DF) transmission electron microscope (TEM) images in **Fig. 7(c)** (Kang *et al.*, 2020a,b; Francois-Saint-Cyr *et al.*, 2019). Specifically, a DF TEM image collected from a base glass with PbSe content of 20 mol% shows sub-wavelength, amorphous secondary phases within an amorphous matrix, as indicated by the bright, circular phases in a dark matrix. The contrast between the secondary phases and the matrix in the DF TEM image suggests that the atomic percentage of heavy constituents in the secondary phases is greater than that in the matrix while the entire nanocomposite remains amorphous. A heat treatment of the base glass with PbSe content of 20 mol% selectively crystallizes the Pb-rich secondary phases, thereby generating high-refractive index nanocrystallites, as indicated by asymmetric shapes of the secondary phases in the DF TEM image. The crystalline fringes existing exclusively within the dark, secondary phases in the high-resolution BF TEM image coherently indicate the emergence of Pb-containing nanocrystals. An increase in the content of PbSe to 40 mol% and a subsequent heat treatment of the composition in the immiscibility zone induces inverse microstructures of the pre- and post-annealed GAP-Se glass with 20 mol% of PbSe. This indicates that the effective index of nanocomposites increases upon heat treatment, while maintaining their transparency as an effective medium. Since the number density and the crystallinity of the high-refractive index, Pb-rich phases can be controlled by knowledge of the nucleation and growth rates of these phases, and thus a prescribed thermal treatment protocol, a combination of the material chemistry and the process leads to our demonstration of a promising method to create a GRIN within a single component. This has been experimentally validated through the use of a gradient heat (growth step) treatment to create a varying number density of Pb-rich phases where the extent of their crystallinity, size, and volume fraction within a glass matrix enables one to spatially tune the effective index of the nanocomposite, as shown in **Fig. 7(d)** (Kang *et al.*, 2020a,b).

Planar GRIN Materials

The GAP-Se material system with lower dimensions has been promising due to its versatility of integration into multi-component structures such as conformal coating as well as its ability to form high refractive index phases. During a thermal evaporation process which has been widely used to deposit ChG films, source materials are condensed on a room temperature or cold substrate. As the

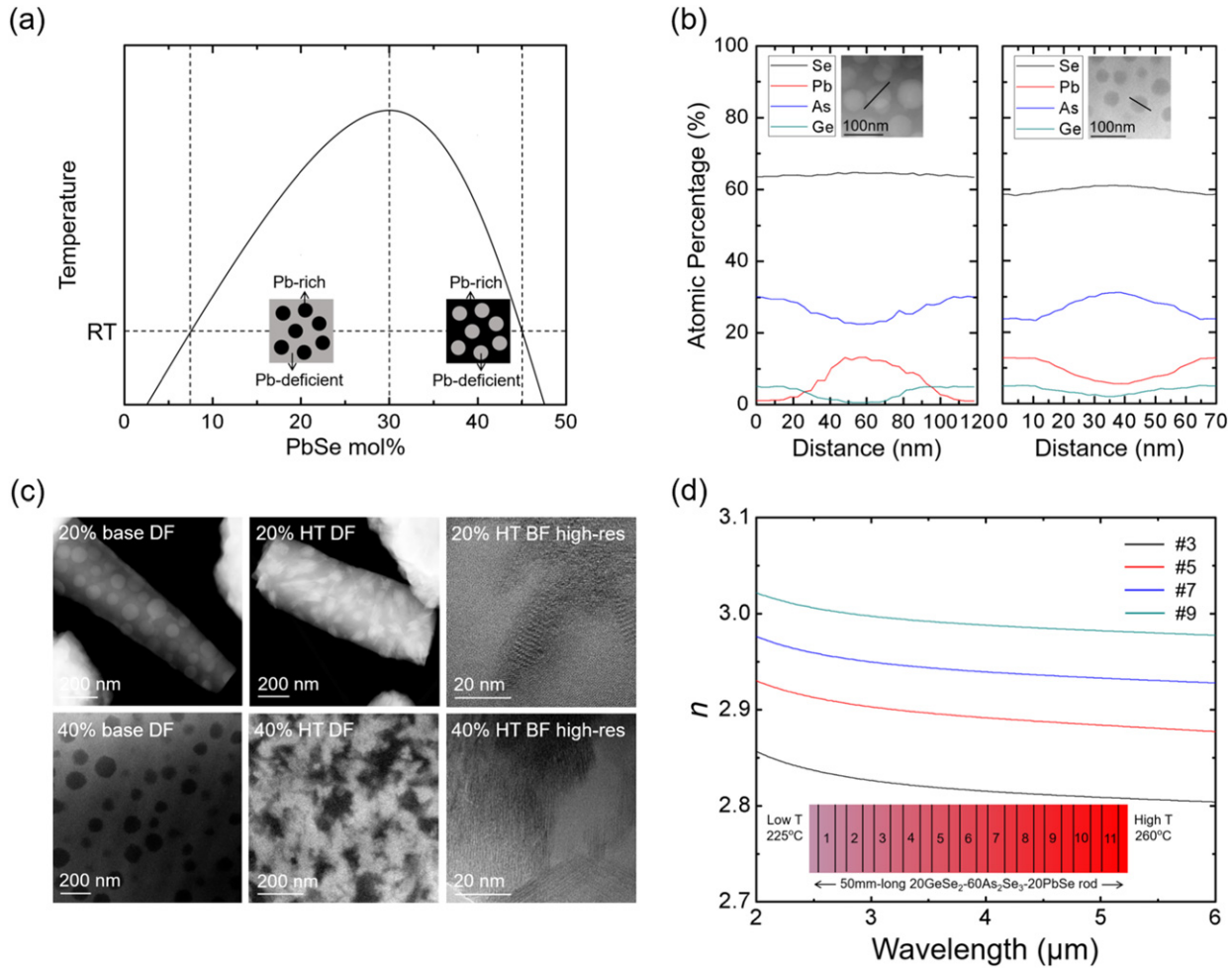

Fig. 7 (a) phase separation of bulk GAP-Se glasses upon standard melt-quench protocol, (b) element segregation across co-existing two phases, (c) microstructures of base glasses and glass-ceramics, (d) GRIN formation in a single bulk glass component. Reproduced with permission from (a) and (b) Goncalves, C., Kang, M., Sohn, B.-U., *et al.*, 2018. New candidate multicomponent chalcogenide glasses for supercontinuum generation. Appl. Sci 8, 2082. Copyright 2018 MDPI. (c) and (d) Kang, M., Sisken, L., Lonergan, C., *et al.*, 2020b. Monolithic chalcogenide optical nanocomposites enable infrared system innovation: Gradient Refractive Index (GRIN) optics. Adv. Opt. Mater. 8, 2000150. Copyright 2020 Wiley.

thermal history in the deposition is energetic, the structure of deposited films remains far from equilibrium and do not typically undergo phase separation upon their deposition; i.e., it remains amorphous with a high concentration of molecular clusters with strained bonds, thereby lowering the activation energy required to transform them to a more stable configuration (Kang *et al.*, 2018a,b, 2019; Mingareev *et al.*, 2019; Mingareev *et al.*, 2020). Therefore, the as-deposited films are energetically metastable and sensitive to external stimulation such as laser exposure and thermal treatment. It has been reported that laser exposure with a wavelength near the optical bandgap energy of the film induces the otherwise homogeneous amorphous structure to be transformed into Pb-rich amorphous phases within a Pb-deficient amorphous matrix (Kang *et al.*, 2018a,b, 2019; Mingareev *et al.*, 2019, 2020). Since the laser exposure-induced Pb-rich amorphous phase is energetically unstable, post heat treatment leads to the conversion of the amorphous phase into Pb-rich nanocrystals with a refractive index far greater than that of the Pb-deficient matrix which still remains amorphous, as shown in **Fig. 8(a)** (Kang *et al.*, 2018a,b). It has been shown that laser exposure can be locally controlled and the laser fluence (power density $\times$ time) dictates the number density of Pb-rich amorphous phases which subsequently become high refractive index nanocrystals upon heat treatment, as illustrated in **Fig. 8(b)** (Kang *et al.*, 2018a,b). The effective refractive index (n_{eff}) of the resulting GC nanocomposite films increases with the volume fraction of the high refractive index nanocrystals. The nanocomposite film's n_{eff} can be approximated by the following equation (Kang *et al.*, 2020a,b):

$$n_{\text{eff}} \approx V_{\text{matrix}} \times n_{\text{matrix}} + \sum_{i=1}^{N} \left(V_{i_{\text{th}}\text{secondary phase}} \times n_{i_{\text{th}}\text{secondary phase}} \right)$$

where n and V correspond to the refractive index and the volume fraction of the nanocomposite's phases, respectively. **Fig. 8(c)** shows that the novel photo-thermal process has been utilized to induce spatially-controlled crystallization within GAP-Se films, thereby realizing a GRIN component such as a diffraction grating structure (Kang *et al.*, 2018a,b).

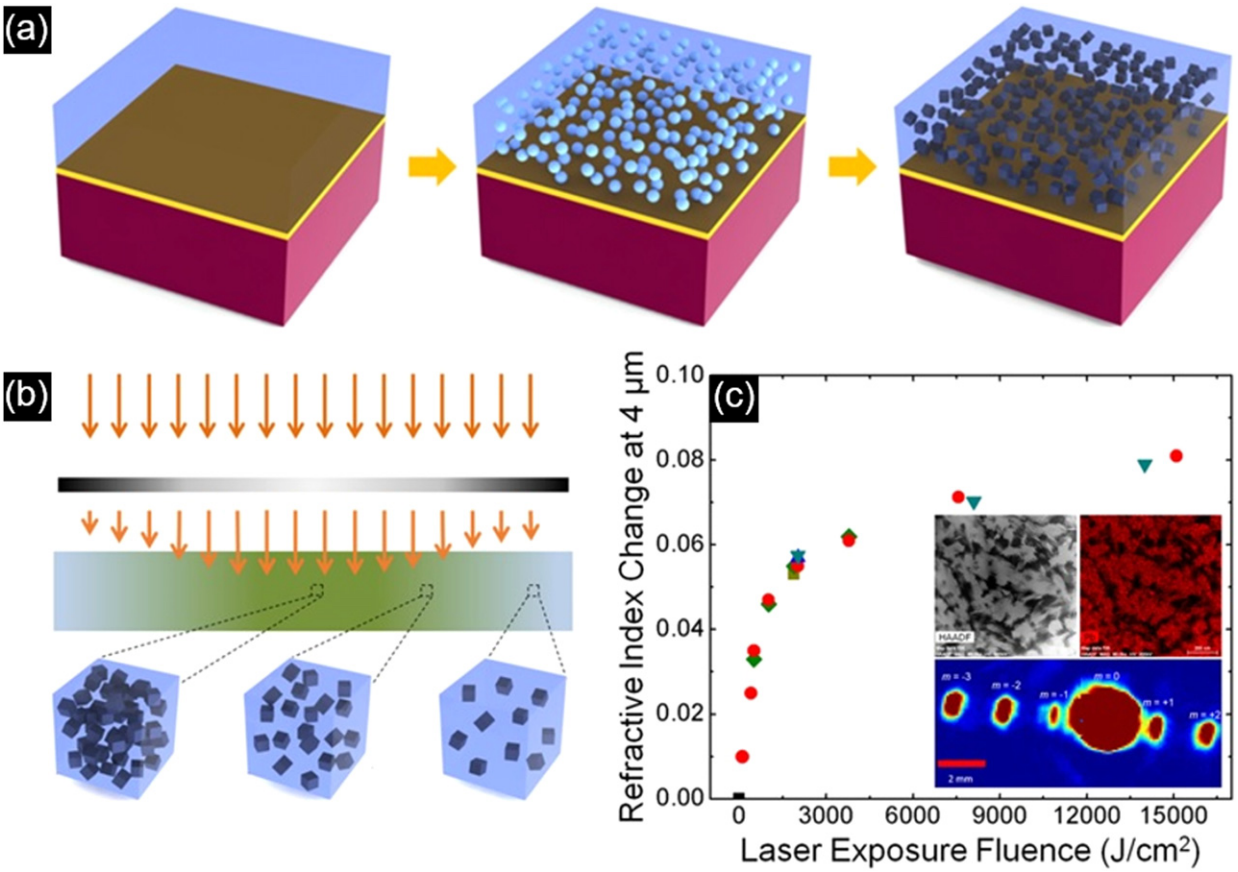

Fig. 8 (a) Film deposition and photo-thermal process leading to the formation of high index nanocrystals within a low index glass matrix, (b) Spatially-controlled laser exposure enabling a GRIN profile, and (c) Utilization of a process-structure-property relationship towards a diffractive GRIN structure. Reproduced with permission from Kang, M., Swisher, A.M., Pogrebnyanov, A.V., *et al.*, 2018b. Ultra-low dispersion multicomponent thin film chalcogenide glass for broadband gradient index optics. Adv. Mater. 30, 1803628. Copyright 2018 Wiley.

Low-Loss Waveguides

Reduction in the ChG material's dimension lends unique nature and planar system design opportunities to the device system. Due to their excellent light confinement, large refractive index, and broadband optical transparency, ChGs such as As_2S_3 and Ge–Sb–S have been actively utilized as optical waveguides, resonators, and interface layers in multi-material micro-photonic systems (Serna *et al.*, 2018; Du *et al.*, 2016; Hu *et al.*, 2007; Xia *et al.*, 2010). Furthermore, their exceptionally high nonlinearity and low multiphoton absorption are ideal for all optical signal processing, allowing ChG-based waveguides to be a core building block of integrated optical circuits (Musgraves *et al.*, 2011). Meanwhile, the most important functionality of waveguides is signal transport with minimum optical loss which has been shown to be as low as a few tenths of dB/cm in some ChG films. One of major sources for the loss is due to optical scattering which can occur from fabrication defects such as sidewall roughness, or where waveguides bend. This phenomenon is presented in a recent work where a series of As_2S_3 waveguides with different bend radii were tested to quantify the optical loss at the bending point, as shown in **Fig. 9(a)–(c)** (Xia *et al.*, 2010). Here, the bend waveguide simulation clearly indicates that the optical loss increases exponentially with decreasing bend radius (i.e., increasing curvature of the waveguide). To mitigate this issue, the addition of a GRIN structure to a bending point of a waveguide has been proposed, as shown in **Fig. 9(d)–(f)** where electric (E_z) and magnetic (H_z) field components of a wave propagating along a silica-based waveguide are observed to maintain their intensities and be confined within the waveguide (Cao *et al.*, 2017).

Optical Nonlinearity

Nonlinear Optical Property Measurements in ChG

The optical nonlinearity of a material significantly depends on the intensity of incident light which in turn is determined by a spacing between a laser beam source and a target material. The z-scan technique utilizes the phenomenon where a target sample is moved along the z-axis to vary incident beam intensity and extract its nonlinear optical parameters, as illustrated in

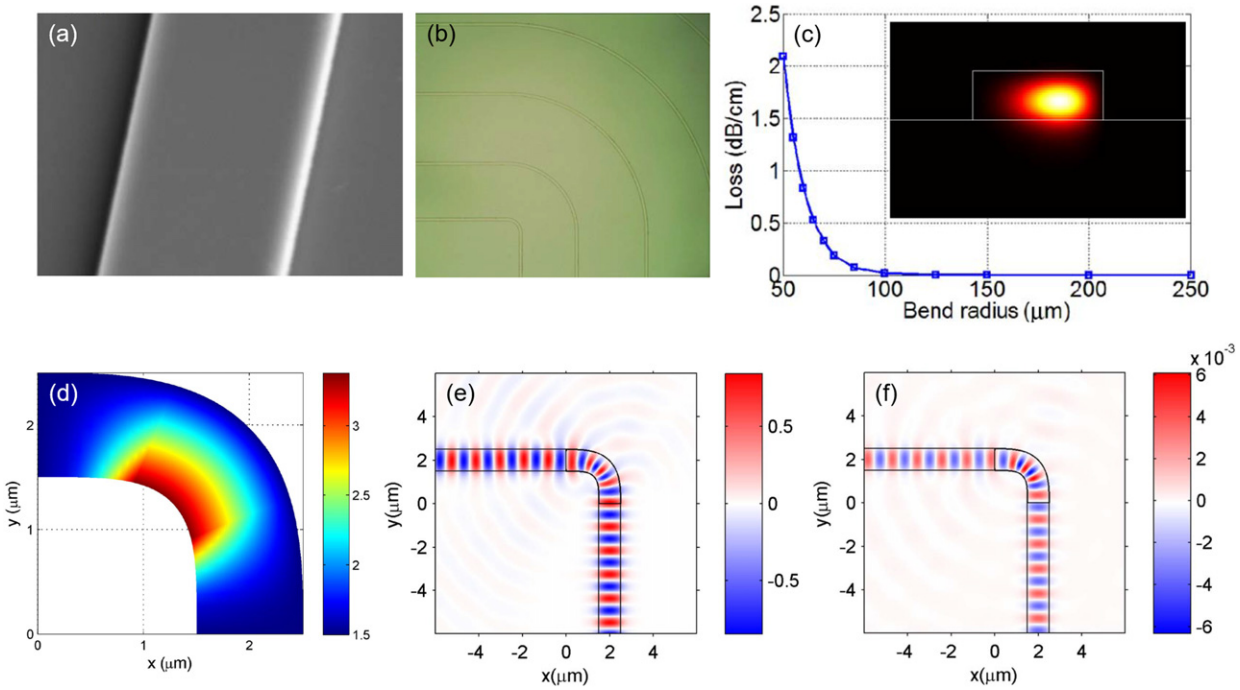

Fig. 9 (a) a SEM image of As_2S_3 waveguides on $LiNbO_3$ substrates, (b) an optical image of the waveguides with different bend radii, (c) optical loss based on bend waveguide simulations, (d) a GRIN structure in silica-based bend waveguides, (e) E_z of the waveguide in TE_0 mode, and (f) H_z of the waveguide in TE_0 mode. Reproduced with permission from (a)–(c) Xia, X., Chen, Q., Tsay, C., Arnold, C.B., Madsen, C.K., 2010. Low-loss chalcogenide waveguides on lithium niobate for the mid-infrared. Opt. Lett. 35, 3228. Copyright 2010 OSA. (d)–(f) reproduced with permission from Cao, Y., Mittra, R., Liu, Z., Zheng, J., 2017. Sharp bend in two-dimensional optical waveguide based on gradient refractive index structure. Appl. Opt. 56, 5336. Copyright 2017 OSA.

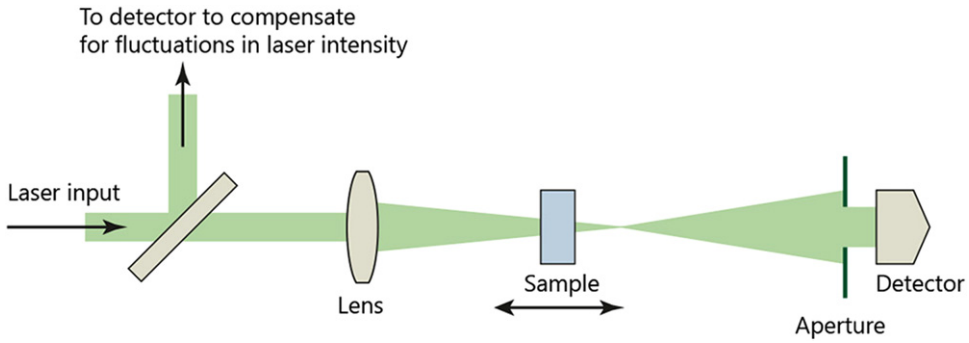

Fig. 10 A schematic of z-scan measurement configuration.

Fig. 10 (Sheik-Bahae *et al.*, 1989, 1991). Specifically, the z-scan technique is used to measure the nonlinear refractive index (n_2) and the nonlinear absorption coefficient (α) to measure both real and imaginary components of the optical nonlinearity. For n_2, a closed-aperture configuration is used. The sample is placed in the focal plane of the lens, and then moved along the (axial) z axis direction, defined by the Rayleigh length. Since the target material reacts like a weak z-dependent lens in this configuration, the far-field aperture makes it possible to detect small distortions in the original beam. The focusing power of this weak nonlinear lens depends on n_2, and therefore it is possible to extract its value by analyzing the z-dependent data acquired by the detector. For α, an open-aperture configuration is used. Specifically, the far-field aperture is removed and the whole signal is measured by the detector. In the whole signal, the small distortions in the original beam are insignificant and the z-dependent signal variation becomes dominant due to the nonlinear multi-photon absorption.

Z-scan is the most common method that has been used to measure n_2 and α for optical materials across a broad spectral window, though new techniques, such as D-scan (Serna *et al.*, 2019, 2018), have been developed for materials in other forms (i.e., planar thin films). Extension of these methods to the spectral window of use relies on an appropriate experimental set up (source/detector) and measurement away from the wavelength of resonance (typically defined as $hv/2$, where hv is the optical bandgap

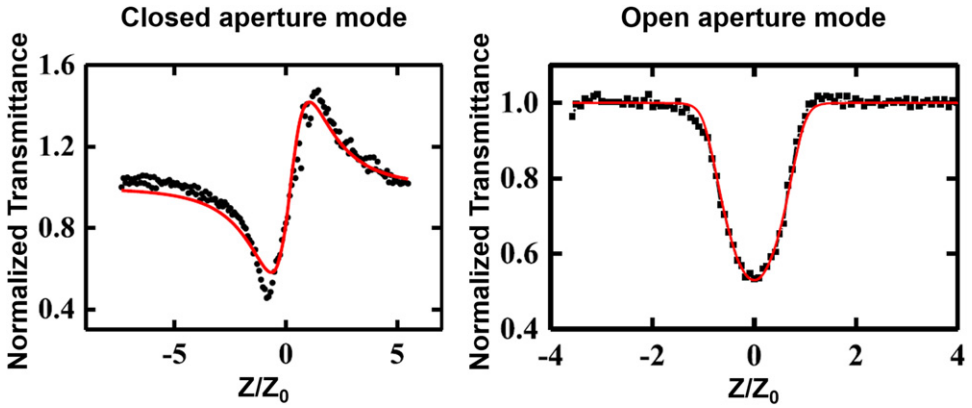

Fig. 11 Closed- and open-modes 4.6 μm z-scan profiles of $Ge_{23}Sb_7S_{70}$ bulk glasses. Reproduced with permission from Sohn, B.-U., Kang, M., Choi, J., *et al.*, 2019. Observation of very high order multi-photon absorption in GeSbS chalcogenide glass. APL Photon. 4, 036102. Copyright 2019 AIP.

energy of the media under test). **Fig. 11** shows representative closed- and open-modes z-scan profiles collected from $Ge_{23}Sb_7S_{70}$ bulk glasses (Sohn *et al.*, 2019). Each set of data includes two types of z-scan measurements including closed and open modes. The z-scan data in the closed mode are fitted with the following equation (Sohn *et al.*, 2017; Wang *et al.*, 2017; Bristow *et al.*, 2007; Kato *et al.*, 1995; Gholami *et al.*, 2011):

$$T_{CA} = 1 + \frac{4\Delta\varphi_0\left(\frac{z}{z_0}\right)}{\left[1+\left(\frac{z}{z_0}\right)^2\right]\left[9+\left(\frac{z}{z_0}\right)^2\right]}$$

where T_{CA}, $\Delta\varphi_0$, z, and z_0 are normalized transmittance in a closed-aperture mode, nonlinear refraction-induced phase change of the laser beam, sample location, and Rayleigh length, respectively. Values of $\Delta\varphi_0$ extracted from a fitted curve are then inserted in the following equation to extract values of nonlinear refractive indices:

$$n_2 = \frac{\Delta\varphi_0\lambda}{2\pi I_{00}L_{eff}}$$

where λ, I_{00}, and L_{eff} are laser wavelength, peak intensity, and effective path length for multiphoton absorption, respectively. The z-scan data in the open mode are fitted with the following equation (Sohn *et al.*, 2017; Wang *et al.*, 2017; Bristow *et al.*, 2007; Kato *et al.*, 1995; Gholami *et al.*, 2011):

$$T_{OA(nPA)} = \frac{1}{\left\{1+(n-1)\alpha_n L_{eff}\left[\frac{I_{00}}{1+\left(\frac{z}{z_0}\right)^2}\right]^{n-1}\right\}^{\frac{1}{n-1}}}$$

where $T_{\text{OA}(n\text{PA})}$, n, α_n correspond to normalized transmittance in an open-aperture mode, integer, and multiphoton absorption coefficient, respectively.

MWIR and LWIR Supercontinuum Generation in ChGs

Here, recent progress on Ge–Sb–S and Ge–Te–AgI based ChGs is introduced as model component behaviors to illustrate compositional variation on optical performance and other variation when formed into fiber. Among ChGs with wide transparency window and large refractive index facilitating mode confinement and bandgap engineering for photonic devices, Ge-based glasses with heavy metal oxide create smaller multiphoton spectra for laser and fiber optic applications (Fuxi, 1992). This phenomenon has necessitated the investigation of Ge-based ternary system's compositional dependence on its optical properties. $Ge_{23}Sb_7S_{70}$ has been demonstrated as one of the promising waveguide materials due to its radiation resistance and lower environmental toxicity as compared to As-based ChGs as well as its broadband optical transparency far into the MWIR spectral region and large optical nonlinearities (Vahalova *et al.*, 2000; Petit *et al.*, 2006; Asami *et al.*, 1997). A recent study utilizes $Ge_{23}Sb_7S_{70}$ waveguides to demonstrate supercontinuum (SC) generation (Choi *et al.*, 2016). **Fig. 12(a)** shows a schematic of $Ge_{23}Sb_7S_{70}$ ridge waveguide fabricated on a SiO_2 substrate where the films were deposited into a patterned substrate using thermal evaporation and tapers at input and output ports in the waveguide to facilitate fiber-waveguide coupling (Choi *et al.*, 2016). To see the evolution of SC generation as a function of input laser peak power (P_{peak}), a femtosecond fiber laser was guided into the $Ge_{23}Sb_7S_{70}$ waveguide. The resulting spectrum broadens from 130 to 320–510–840 nm at -30 dB level as P_{peak} increases from 120 to 220–280–340 W, respectively, as shown in **Fig. 12(b)** (Choi *et al.*, 2016). The remarkably large spectral broadening of 900 nm shows that GeSbS waveguides with a relatively large nonlinear parameter and negligible nonlinear losses could be a promising platform for

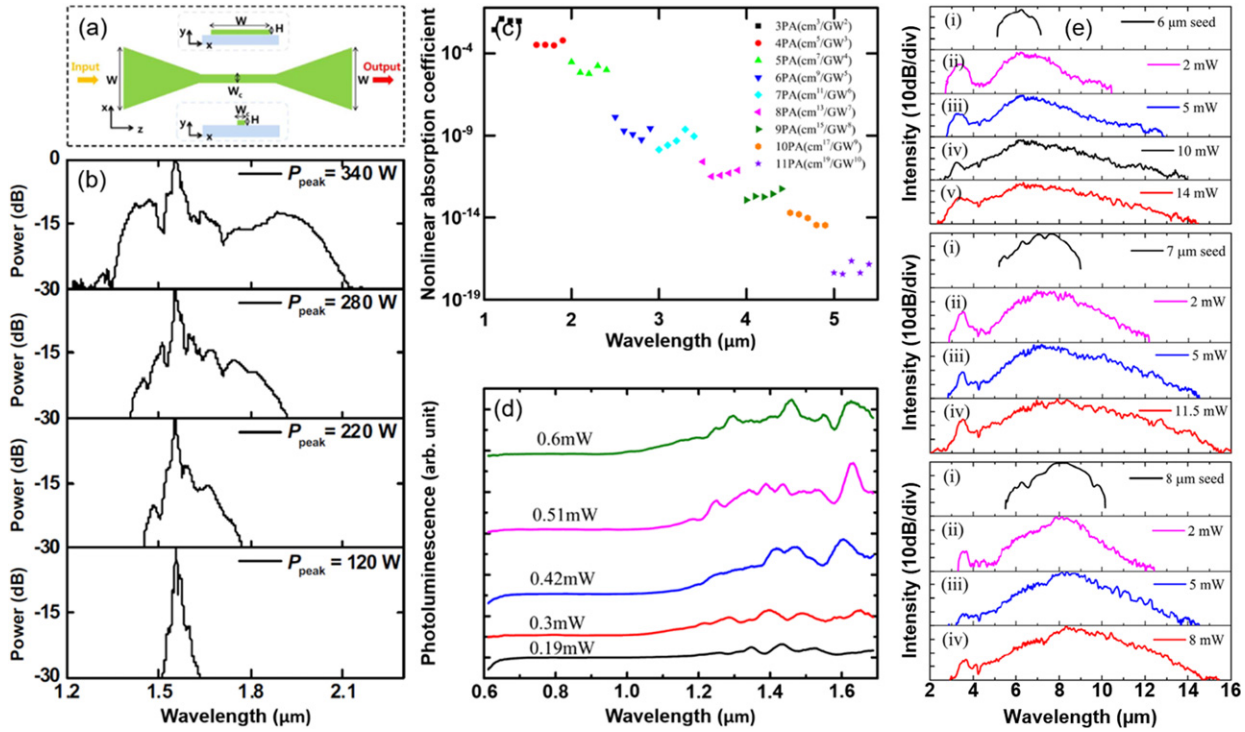

Fig. 12 (a) Schematic of $Ge_{23}Sb_7S_{70}$ waveguide (sky color: SiO_2 substrate, light green color: $Ge_{23}Sb_7S_{70}$ film), (b) output SC spectrum in $Ge_{23}Sb_7S_{70}$ waveguide as a function of input peak power, (c) multiphoton absorption coefficients of $Ge_{23}Sb_7S_{70}$ bulk glasses in the range 1.1–5.5 μm, (d) photoluminescence of $Ge_{23}Sb_7S_{70}$ bulk glasses induced by four-photon absorption. (e) experimental SC spectra pumped at 6, 7, and 8 μm in a step-index fiber consisting of $(Ge_{10}Te_{43})_{90}$-$(AgI)_{10}$ core with two claddings including $(Ge_{10}Te_{40})_{90}$-$(AgI)_{10}$ and $Ge_{10}Sb_{10}Se_{80}$. Reproduced with permission from (a) and (b) Choi, J., Han, Z., Sohn, B., *et al.*, 2016. Nonlinear characterization of GeSbS chalcogenide glass waveguides. Sci. Rep. 6, 39234. Copyright 2016 Springer Nature. (c) and (d) reproduced with permission from Sohn, B.-U., Kang, M., Choi, J., *et al.*, 2019. Observation of very high order multi-photon absorption in GeSbS chalcogenide glass. APL Photon. 4, 036102. Copyright 2019 AIP. (e) reproduced with permission from Zhao, Z., Wu, B., Wang, X., *et al.*, 2017. Mid-infrared supercontinuum covering 2.0–16 mm in a low-loss telluride single-mode fiber. Laser Photon. Rev. 11, 1700005. Copyright 2017 Wiley.

nonlinear optics applications at telecommunication wavelengths. Meanwhile, despite the implications from the nonlinear figure of merit, it is not always the case that the real part of the nonlinear susceptibility is the only factor worth maximizing for optical applications. The imaginary part of the nonlinear susceptibility is likewise important in that it can be utilized for photodetection, nonlinearly generated light sources, and band-structure identification (Sohn *et al.*, 2019; Zhao *et al.*, 2017). In this context, multiphoton absorption behavior and resulting photoluminescence (PL) of $Ge_{23}Sb_7S_{70}$ bulk glasses have been recently studied as shown in **Fig. 12(c)** and **(d)**. **Fig. 12(c)** shows up to eleven-photon absorptions which is by far the highest order multiphoton absorption experimentally recorded to date (Sohn *et al.*, 2019). Such understanding of inter-band gap energy transition levels is crucial in applications such as SC or high harmonic generation where high pump intensities are required, since sub-bandgap excitation wavelength is much preferred to avoid any radiation-induced structural modification. **Fig. 12(d)** shows the PL signal observed between 1.1 and 1.68 μm, with its intensity increasing with the incident pump power (Sohn *et al.*, 2019). The slope obtained between the PL signal and input intensity was extracted to be 3.9, which is very close to the integer 4, implying that the PL is associated with four-photon absorption. The results pave the way towards new photonic device design leveraging very high order multiphoton absorption effects and multiphoton-excited PL. Meanwhile, the replacement of a light element for a heavier one typically enhances the optical nonlinearity of the materials (Wang, 2014) and broadens their optical transparency window (Wilhelm *et al.*, 2007). Especially, telluride glasses have been reported to possess the highest optical nonlinearity and broadest transmission window (Wilhelm *et al.*, 2007). Also, Se–Se induced multiphoton absorption, known to limit the broadening of SC spectra of telluride glasses, has been overcome by several candidate systems such as Ge–Te–I (Wilhelm *et al.*, 2007), Ge–Ga–Te (Danto *et al.*, 2006), and Ge–Te–AgI (Wang *et al.*, 2012; Conseil *et al.*, 2012) without containing Se. For iodine-containing tellurides, the high atomic weight of iodine allows the glass matrix's low phonon character to be maintained, thereby retaining the far-IR transparency. Furthermore, the nonlinearity of tellurides has been known to be further improved by doping with Cu or Ag (Ogusu and Shinkawa, 2009) and, based upon aforementioned findings, the Ge–Te–AgI glass system has been promising for fiber drawing and SC generation in the MWIR. **Fig. 12(e)** shows SC spectra excited by different pump wavelengths at 6, 7, and 8 μm in a $(Ge_{10}Te_{43})_{90}$-$(AgI)_{10}$ fiber (Zhao *et al.*, 2017). At each pumping wavelength, the SC spectrum broadens as the pump power increases. The SC spectra are extended to 14.5, 16, and 15.4 μm under maximum pump power at different pump wavelengths of 6,

Table 1 Experimental MWIR SC generation in the ChG fiber (more than 12 μm)

Fiber	*Fiber length (cm)*	*ZDW (μm)*	*Pump wavelength (μm)*	*SC bandwidth (μm)*
As-Se	8.5	5.83	6.3	1.4–13.3 (30 dB)
As-Se	3	5.5	9.8	2–15.1 (–)
Ge–Sb–Se	20	5.5	6	1.8–14 (–)
Ge–As–Se–Te	23	10.5	4.5	1.5–14 (30 dB)
Ge–Te–AgI	14	10.5	7	2–16 (40 dB)

Note: Reproduced with permission from Zhao, Z., Wu, B., Wang, X., *et al.*, 2017. Mid-infrared supercontinuum covering 2.0–16 mm in a low-loss telluride single-mode fiber. Laser Photon. Rev. 11, 1700005. Copyright 2017 Wiley.

7, and 8 μm, respectively. **Table 1** tabulates the experimental SC data generated in a variety of ChG fibers where Te-based fibers have a broader transparent window than other ChG fibers, making them suitable for SC generation in the MWIR (Zhao *et al.*, 2017).

Summary

The key material attributes of chalcogenide glass and glass ceramic materials aimed at enabling their use in a variety of IR applications is presented. The ability to control and utilize the glass' composition, microstructure (where a glass ceramic is formed), and the material's resulting optical properties in bulk, film, fiber, and waveguide forms is reviewed. Also discussed are lingering issues that remain as challenges to the community in translating these glasses into these forms, including relevant microstructural and optical metrology methods which have been used to assess them. The effort and progress made by the glass science and engineering community as well as the optical design and fabrication "users" of the glasses has advanced considerably since the turn of the century. These efforts will likely continue as researchers and manufacturers evaluate and develop strategies to further optimize properties suitable for higher volume applications. Such work will enable chalcogenide glasses for use in a diverse range of applications and highlight the promising future of these novel materials in next generation optical systems and beyond.

References

Adam, J.L., Zhang, X., 2014. Chalcogenide Glasses: Preparation, Properties and Applications. Woodhead Publishing Limited.

Asami, T., Matsuishi, K., Onari, S., Arai, T., 1997. Low frequency Raman scattering spectra of $(GeS_2)_{1-x}(Sb_2S_3)_x$ amorphous semiconductors. J. Non-Cryst. Solids 211, 89.

Beadie, G., Rabinovich, W.S., Sanghera, J., Aggarwal, I., 1998. Fabrication of microlenses in bulk chalcogenide glass. Opt. Commun. 152, 215.

Bixby W.E., Ullrich O.A., 1956. Method for the production of a photographic plate, U.S. Patent 2,753,278.

Booth, M.J., 2014. Adaptive optical microscopy: The ongoing quest for a perfect image. Light Sci. Appl 3. e165.

Bristow, A., Rotenberg, N., van Driel, H., 2007. Two-photon absorption and Kerr coefficients of silicon for 850–2200 nm. Appl. Phys. Lett. 90.191104

Buff, A.K., 2016. A Study of Crystallization Behavior in Phase Separated Chalcogenide Glasses. Master Thesis. University of Central Florida.

Cao, Y., Mittra, R., Liu, Z., Zheng, J., 2017. Sharp bend in two-dimensional optical waveguide based on gradient refractive index structure. Appl. Opt. 56, 5336.

Carlie, N., Musgraves, J.D., Zdyrko, B., *et al.*, 2010. Integrated chalcogenide waveguide resonators for mid-IR sensing: leveraging material properties to meet fabrication challenges. Opt. Express 18, 26728.

Cha, D.H., Kim, H., Hwang, Y., Jeong, J.C., Kim, J., 2012. Fabrication of molded chalcogenide-glass lens for thermal imaging applications. Appl. Opt. 51, 5649.

Choi, J., Han, Z., Sohn, B., *et al.*, 2016. Nonlinear characterization of GeSbS chalcogenide glass waveguides. Sci. Rep. 6. 39234.

Conseil, C., Bastien, J.C., Boussard-Pledel, C., *et al.*, 2012. Te-based chacohalide glasses for far-infrared optical fiber. Opt. Mater. Express 2, 1470.

Danto, S., Houizot, P., Boussard-Pledel, C., *et al.*, 2006. A family of far-infrared-transmitting glasses in the Ga-Ge-Te system for space applications. Adv. Funct. Mater. 16, 1847.

Dianov, E.M., Shiryaev, V.S., Izyneev, A.A., Plotnichenko, G.E., Charbanov, M.F., 1997. Crystallization kinetics of praseodymium-doped $(Ga_2S_3)_{0.7}(La_2S_3)_{0.3}$ glass. Inorg. Mater. 33, 975.

Du, Q., Huang, Y., Li, J., *et al.*, 2016. Low-loss photonic device in Ge-Sb-S chalcogenide glass. Opt. Lett. 41, 3090.

Eggleton, B.J., Luther-Davies, B., Richardson, K.A., 2011. Chalcogenide photonics. Nat. Photon. 5, 141.

Francois-Saint-Cyr, H., Kang, M., Martin, I., *et al.*, 2019. Three-dimensional microstructural characterization of novel chalcogenide nanocomposites for gradient refractive index applications. Microsc. Microanal. 25, 2500.

Fuxi, G., 1992. Structure, properties and applications of chalcohalide glasses: A review. J. Non-Cryst. Solids 140, 184.

Gholami, F., Zlatanovic, S., Simic, A., *et al.*, 2011. Third-order nonlinearity in silicon beyond 2350 nm. Appl. Phys. Lett. 99. 081102.

Gibson, D., Bayya, S., Nguyen, V., *et al.*, 2019. Multispectral IR optics and GRIN. In: Proceedings of the SPIE, vol. 10998, 10998-12.

Goncalves, C., Kang, M., Sohn, B.-U., *et al.*, 2018. New candidate multicomponent chalcogenide glasses for supercontinuum generation. Appl. Sci 8, 2082.

Hari, P., Taylor, P.C., King, W.A., LaCourse, W.C., 1998. Metastable, drawing-induced crystallization in As_2Se_3 fibers. J. Non-Cryst. Solids 227, 789.

Hilton, A.R., 2010. Chalcogenide Glasses for Infrared Optics. McGraw Hill.

Hisakuni, H., Tanaka, K., 1995. Optical fabrication of microlenses in chalcogenide glasses. Opt. Lett. 20, 958.

Hu, J., Tarasov, V., Agarwal, A., *et al.*, 2007. Fabrication and testing of planar chalcogenide waveguide integrated microfluidic sensor. Opt. Express 15, 2307.

Kang, M., Sisken, L., Cook, J., *et al.*, 2018a. Refractive index patterning of infrared glass ceramics through laser-induced vitrification. Opt. Mater. Express 8, 2722.

Kang, M., Swisher, A.M., Pogrebnyanov, A.V., *et al.*, 2018b. Ultra-low dispersion multicomponent thin film chalcogenide glass for broadband gradient index optics. Adv. Mater. 30. 1803628.

Kang, M., Malendevych, T., Yin, G., *et al.*, 2019. Scalable laser-written Ge-As-Pb-Se chalcogenide glass-ceramic films and the realization of infrared gradient refractive index elements. In: Proceedings of the SPIE, vol. 10998, 109980E-1.

Kang, M., Francois-Saint-Cyr, H., Martin, I., *et al*., 2020a. Unveiling true three-dimensional microstructural evolution in novel chalcogenide nanocomposites as a route to infrared gradient refractive index functionality. Microsc. Microanal. (In press).
Kang, M., Sisken, L., Lonergan, C., *et al*., 2020b. Monolithic chalcogenide optical nanocomposites enable infrared system innovation: Gradient Refractive Index (GRIN) optics. Adv. Opt. Mater. 8. 2000150.
Kato, T., Suetsugu, Y., Takagi, M., Sasaoka, E., Nishimura, M., 1995. Measurements of the nonlinear refractive index in optical fiber by the cross-phase-modulation method with depolarized pump light. Opt. Lett. 20, 988.
Kokorina, V.F., 1996. Glasses for Infrared Optics. CRC Press.
Kolobov, A.V., Tanaka, K., 2001. Photoinduced phenomena in amorphous chalcogenides: from phenomenology to nanoscale. In: Nalwa, H.S. (Ed.), Handbook of Advanced Electronic and Photonic Materials and Devices. Academic Press.
Kolobov, A.V., Tominaga, J., 2012. Chalcogenides: Metastability and Phase Change Phenomena. Springer.
Koontz, E., 2014. Characterization of Structural Relaxation in Inorganic Glasses Using Length Dilatometry. PhD Dissertation. Clemson University.
Kumaresan, Y., Rammohan, A., Dwivedi, P.K., Sharma, A., 2013. Large area ir microlens arrays of chalcogenide glass photoresists by grayscale maskless lithography. ACS Appl. Mater. Interfaces 5, 7094.
Li, H.H., 1980. Refractive index of silicon and germanium and its wavelength and temperature derivatives. J. Phys. Chem. Ref. Data 9, 561.
Li, L., Lin, H., Qiao, S., *et al*., 2014. Integrated flexible chalcogenide glass photonic devices. Nat. Photon. 8, 643.
Martin, S.W., Bloyer, D.R., 1990. Preparation of high-purity vitreous B_2S_3. J. Am. Ceram. Soc. 73, 3481.
Massera, J., 2009. Nucleation and Growth of Tellurite-Based Glasses Suitable for Mid-infrared Applications. PhD Dissertation. Clemson University.
Massera, J., Haldeman, A., Milanese, D., *et al*., 2010a. Processing and characterization of a core-clad tellurite glass preforms and fibers fabricated by rotational casting. J. Opt. Mater. 32, 582.
Massera, J., Remond, J., Musgraves, J.D., *et al*., 2010b. Nucleation and growth behavior of glasses in the TeO_2-Bi_2O_3-ZnO glass system. J. Non-Cryst. Solids 356, 2947.
Mauro, J.C., Tandia, A., Vargheese, K.D., Mauro, Y.Z., Smedskjaer, M.M., 2016. Accelerating the design of functional glasses through modeling. Chem. Mater. 28, 4267.
Mikhailov, M.D., Tver'yanovick, A.S., 1986. Critical cooling rates of chalcogenide glass-forming melts. Fizika I Khimiya Stekla 12, 274.
Mingareev, I., Kang, M., Malendevych, T., *et al*. 2019. Laser-induced modification of local refractive index in infrared glass-ceramic films. In: Proceedings of the SPIE, vol. 10906, 109060X.
Mingareev, I., Kang, M., Truman, M., *et al*., 2020. Spatial tailoring of the refractive index in infrared glass-ceramic films enabled by direct laser writing. Opt. Laser Technol. 126. 106058.
Moore, D.T., 1980. Gradient-index optics: A review. Appl. Opt. 19, 1035.
Musgraves, J.D., Wachtel, P., Novak, S., Wilkinson, J., Richardson, K., 2011. Composition dependence of the viscosity and other physical properties in the arsenic selenide glass system. J. Appl. Phys. 110. 063503.
Ogusu, K., Shinkawa, K., 2009. Optical nonlinearities in As_2Se_3 chalcogenide glasses doped with Cu and Ag for pulse durations on the order of nanoseconds. Opt. Express 17, 8165.
Parvanov, S., Vassilev, V., Tomova, K., 2008. Optical properties of new chalcogenide glasses from the $GeSe_2$-Sb_2Se_3-PbSe system. Mater. Lett. 62, 2021.
Petit, L., Carlie, N., Richardson, K.C., *et al*., 2006. Correlation between physical, optical and structural properties of sulfide glasses in the system Ge-Sb-S. Mater. Chem. Phys. 97, 64.
Ramachandran, S., Pepper, J.C., Brady, D.J., Bishop, S.G., 1997. Micro-optical lenslets by photo-expansion in chalcogenide glasses. J. Lightwave Technol. 15, 1371.
Richardson, K., Kang, M., 2020. Chalcogenide materials for mid-wave infrared fiber. In: Jackson, S., Vallee, R., Bernier, M. (Eds.), Mid-Infrared Fibre Photonics. Elsevier.
Richardson, K., Buff, A., Smith, C., *et al*., 2016. Engineering novel infrared glass ceramics for advanced optical solutions. In: Proceedings of the SPIE, vol. 9822, 982205.
Richardson, K., Kang, M., Sisken, L., *et al*. 2018. Advances in infrared GRIN: A review of novel materials towards components and devices. In: Proceedings of the SPIE, vol. 10627, 106270A.
Saitoh, A., Tanaka, K., 2003. Self-developing aspherical chalcogenide-glass microlenses for semiconductor lasers. Appl. Phys. Lett. 84, 1725.
Sanchez, E.A., Waldmann, M., Arnold, C.B., 2011. Chalcogenide glass microlenses by inkjet printing. Appl. Opt. 50, 1974.
Sanghera, J.S., Aggarwal, I.D., 1999. Active and passive chalcogenide glass optical fibers for IR applications: A review. J. Non-Cryst. Solids 256, 6.
Seddon, A.B., Pan, W.J., Furniss, D., *et al*., 2006. Fine embossing of chalcogenide glasses – A new fabrication route for photonic integrated circuits. J. Non-Cryst. Solids 352, 2515.
Serna, S., Lin, H., Alonso-Ramos, C., *et al*., 2018. Nonlinear optical properties of integrated GeSbS chalcogenide waveguides. Photon. Res. 6, B37.
Serna, S., Lin, H., Alonso-Ramos, C., *et al*., 2019. Engineering third order optical nonlinearities in hybrid chalcogenides-on-silicon platform. Opt. Lett. 44, 5009.
Sharma, R., Welch, R., Kang, M., *et al*., 2020. Impact of morphology and microstructure on the mechanical properties of Ge-As-Pb-Se glass ceramics. Appl. Sci. 10, 2836.
Sheik-Bahae, M., Said, A.A., van Stryland, E.W., 1989. Sensitive measurement of optical nonlinearities using a single beam. Opt. Lett. 14, 955.
Sheik-Bahae, M., Hutchings, D.C., Hagan, D.J., van Stryland, E.W., 1991. Dispersion of bound electron nonlinear refraction in solids. IEEE J. Quantum Electron. 27, 1296.
Shiryaev, V.S., Adam, J.-L., Zhang, X.H., 2004. Calorimetric study of characteristic temperatures and crystallization behaviour in Ge-As-Se-Te glass system. J. Phys. Chem. Solids 65, 1737.
Sisken, L., 2017. Laser-Induced Crystallization Mechanisms in Chalcogenide Glass Materials for Advanced Optical Functionality. PhD Dissertation. University of Central Florida.
Sisken, L., Kang, M., Veras, J.M., *et al*., 2019. Infrared glass ceramics with multi-dispersion and gradient refractive index attributes. Adv. Funct. Mater. 29. 1902217.
Sohn, B.-U., Kang, M., Choi, J., *et al*., 2019. Observation of very high order multi-photon absorption in GeSbS chalcogenide glass. APL Photon. 4. 036102.
Sohn, B.-U., Monmeyran, C., Kimerling, L.C., Agarwal, A.M., Tan, D.T.H., 2017. Kerr nonlinearity and multi-photon absorption in germanium at mid-infrared wavelengths. Appl. Phys. Lett. 111. 091902.
Texas Instruments, 1967. Multi-component chalcogenide glass compositions, US3338728A (Ge-P-Te), US3343972A (Ge-Te-As) and US3360649A (Ge-Sb-S).
Tikhomirov, V.K., Furniss, D., Seddon, A.B., *et al*., 2004. Glass formation in the Te-enriched part of the quaternary Ge-As-Se-Te system and its implication for mid-infrared optical fibres. Infrared Phys. Technol. 45, 115.
Vahalova, R., Tichy, L., Vlcek, M., Ticha, H., 2000. Far infrared spectra and bonding arrangement in some Ge-Sb-S glasses. Phys. Status Solidi A 181, 199.
Wang, H., Zhang, X., Yang, G., *et al*., 2009. Micro-crystallization of the infrared transmitting chalcogenide glass in $GeSe_2$-As_2Se_3-PbSe system. Ceram. Int. 35, 83.
Wang, R., 2014. Amorphous Chalcogenides: Advances and Applications. Pan Stanford Publishing.
Wang, T., Venkatram, N., Gosciniak, J., *et al*., 2017. Multi-photon absorption and third-order nonlinearity in silicon at mid-infrared wavelengths. Opt. Express 21, 32192.
Wang, X., Nie, Q., Wang, G., *et al*., 2012. Investigation of Ge-Te-AgI chalcogenide glass for far-infrared application. Spectrochim. Acta. A: Mol. Biomol. Spectrosc. 86, 586.
Wilhelm, A.A., Boussard-Pledel, C., Coulombier, Q., *et al*., 2007. Development of far-infrared-transmitting Te based glasses suitable for carbon dioxide detection and space optics. Adv. Mater. 19, 3796.
Xia, F., Zhang, X., Ren, J., *et al*., 2006. Glass formation and crystallization behavior of a novel GeS_2-Sb_2S_3-PbS chalcogenide glass system. J. Am. Ceram. Soc. 89, 2154.
Xia, X., Chen, Q., Tsay, C., Arnold, C.B., Madsen, C.K., 2010. Low-loss chalcogenide waveguides on lithium niobate for the mid-infrared. Opt. Lett. 35, 3228.
Yadav, A., Kang, M., Smith, C., *et al*., 2017. Influence of phase separation on structure-property relationships in the $(GeSe_2\text{-}3As_2Se_3)_{1-x}PbSe_x$ glass system. Phys. Chem. Glasses 58, 115.
Yadav, A., Buff, A., Kang, M., *et al*., 2019. Melt property variation in $GeSe_2$-As_2Se_3-PbSe glass ceramics for infrared gradient refractive index (GRIN) applications. Int. J. Appl. Glass Sci. 10, 27.
Yang, G., Zhang, X., Ren, J., *et al*., 2007. Glass formation and properties of chalcogenide in a $GeSe_2$-As_2Se_3-PbSe system. J. Am. Ceram. Soc. 90, 1500.

Zhang, X.H., Guimond, Y., Bellec, Y., 2003. Production of complex chalcogenide glass optics by molding for thermal imaging. J. Non-Cryst. Solids 326, 519.
Zhang, X.H., Ma, H., Lucas, J., 2004. Evaluation of glass fibers from the Ga-Ge-Sb-Se system for infrared applications. Opt. Mater. 25, 85.
Zhang, Y., Chou, J.B., Li, J., *et al*., 2019. Broadband transparent optical phase change materials for high-performance nonvolatile photonics. Nat. Commun. 10, 4279.
Zhao, D., Xia, F., Chen, G., *et al*., 2005. Formation and properties of chalcogenide glasses in the $GeSe_2$-As_2Se_3-CdSe system. J. Am. Ceram. Soc. 88, 3143.
Zhao, Z., Wu, B., Wang, X., *et al*., 2017. Mid-infrared supercontinuum covering 2.0–16 μm in a low-loss telluride single-mode fiber. Laser Photon. Rev. 11. 1700005.